Supporting Information

Microsphere Autolithography—a Scalable Approach for Arbitrary Patterning of Dielectric Spheres

Elliott D. Kunkel, Alec G. Burnett, Katherine E. Scheiber, and Hans D. Robinson*

Department of Physics, Virginia Tech, Blacksburg, Virginia 24061

*E-mail: hansr@vt.edu

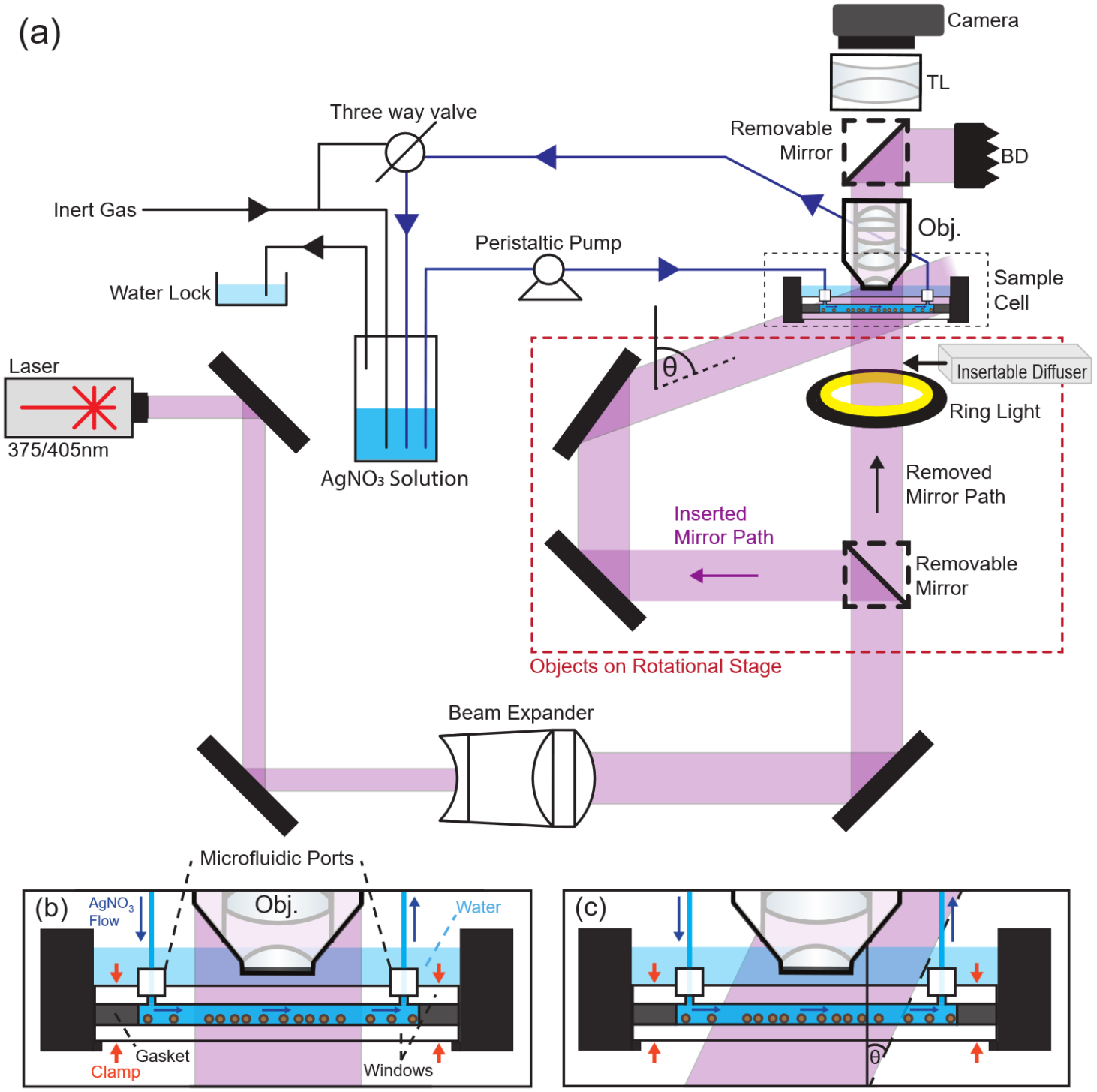

Figure S1: (a) Experimental setup and optical exposure scheme. A deoxygenated silver nitrate solution is continuously purged with inert gas and circulated through the sample cell using a peristaltic pump. Light from the exposing laser is expanded and directed onto the sample either through the inserted mirror path or the removed mirror path, enabling illumination at both normal to the sample, and and at an oblique incidence angle θ. Exposed samples can be imaged in situ through the water immersion microscope objective after exposure by inserting a diffuser below the sample and turning on the ring light, which produces a uniform illumination of the sample from below. (b) Normal exposure through removed mirror path. (c) Oblique exposure through the inserted mirror path, where the azimuthal angle can be varied with the Rotation Stage.

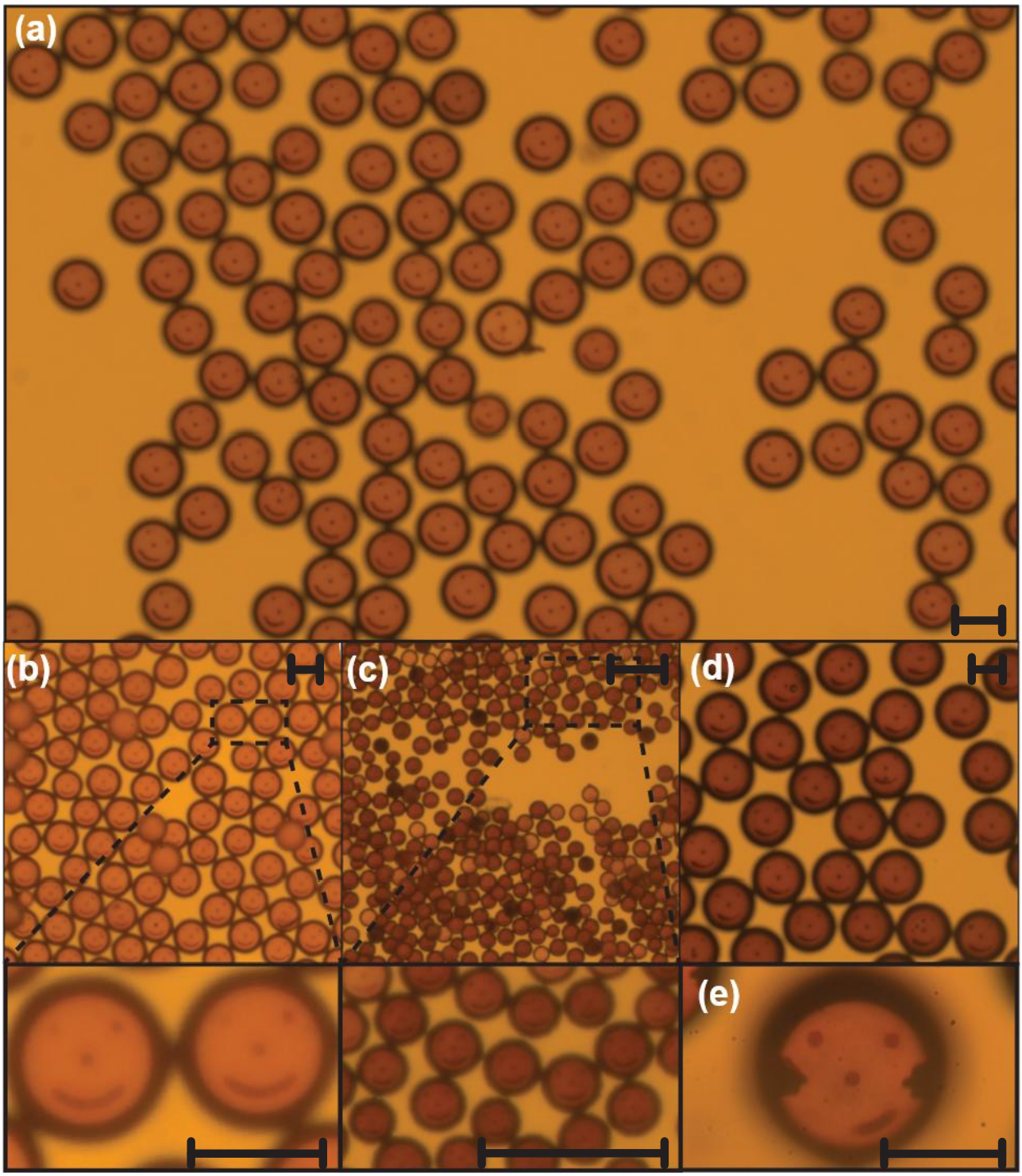

Figure S2: Metal silver "smiley" patterns on BTG microspheres. (a,b) $n_2 \sim 2.2$ particles, ∅ = 56–66 μm. (c) $n_2 \sim 2.2$ particles, ∅ = 10–22 μm. (d), (e) $n_2 \sim 2.2$ particles, ∅ = 78–85 μm. The crooked "smiles" are due to misalignment of the exposing laser beam. The "ear"-like features in (e) are shadows of microfluidic ports present in an earlier version of the microfluidic cell.

All particles were coated with PDA and exposed to 405 nm wavelength light in a 50 mM $AgNO_3$ aqueous solution. The scale bars are 50 μm.

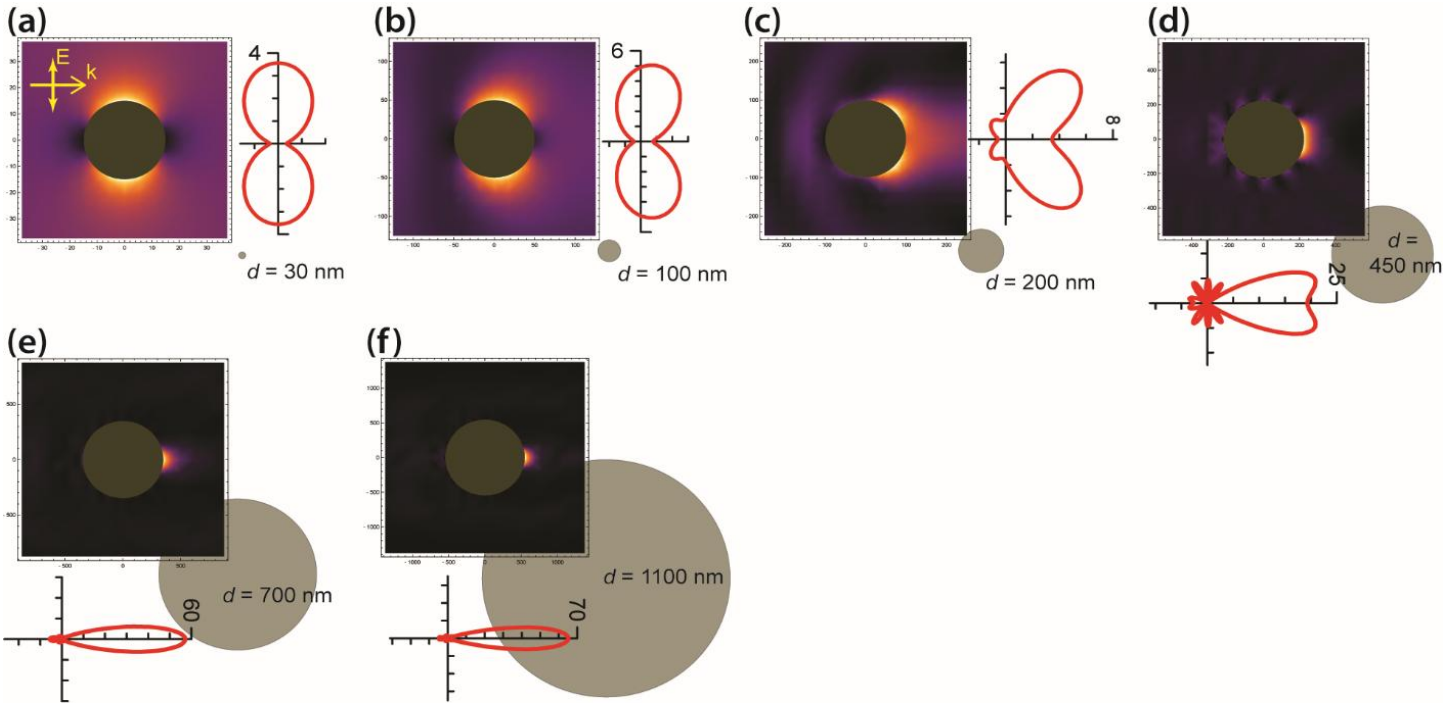

Figure S3: Mie scattering calculations of a plane wave (entering from the left, vertically polarized in the plane of the page) with $\lambda = 450$ nm scattering off titania spheres suspended in a solvent with $n_1 = 1.44$. Particle diameters are (a) 30 nm, (b) 100 nm, (c) 200 nm, (d) 450 nm, (e) 700 nm, and (f) 1100 nm. The intensity plots show electromagnetic intensity on a cross-section through the sphere centers in the near-field of the particles. The polar plots also show near-field intensity, measured 1 nm off the surface of the sphere, with the scale in multiples of the intensity of the incident light. The discs on the lower right of each panel indicate the relative sizes of the spheres.

For the smallest particles, the illumination produces two patches around the poles of the spheres. As particle size is increased, retardation effects shift the patches in the direction of propagation until they merge into a single spot for particle sizes of approximately 0.5 μm, when the light distribution becomes qualitatively consistent with the predictions of geometric optics.

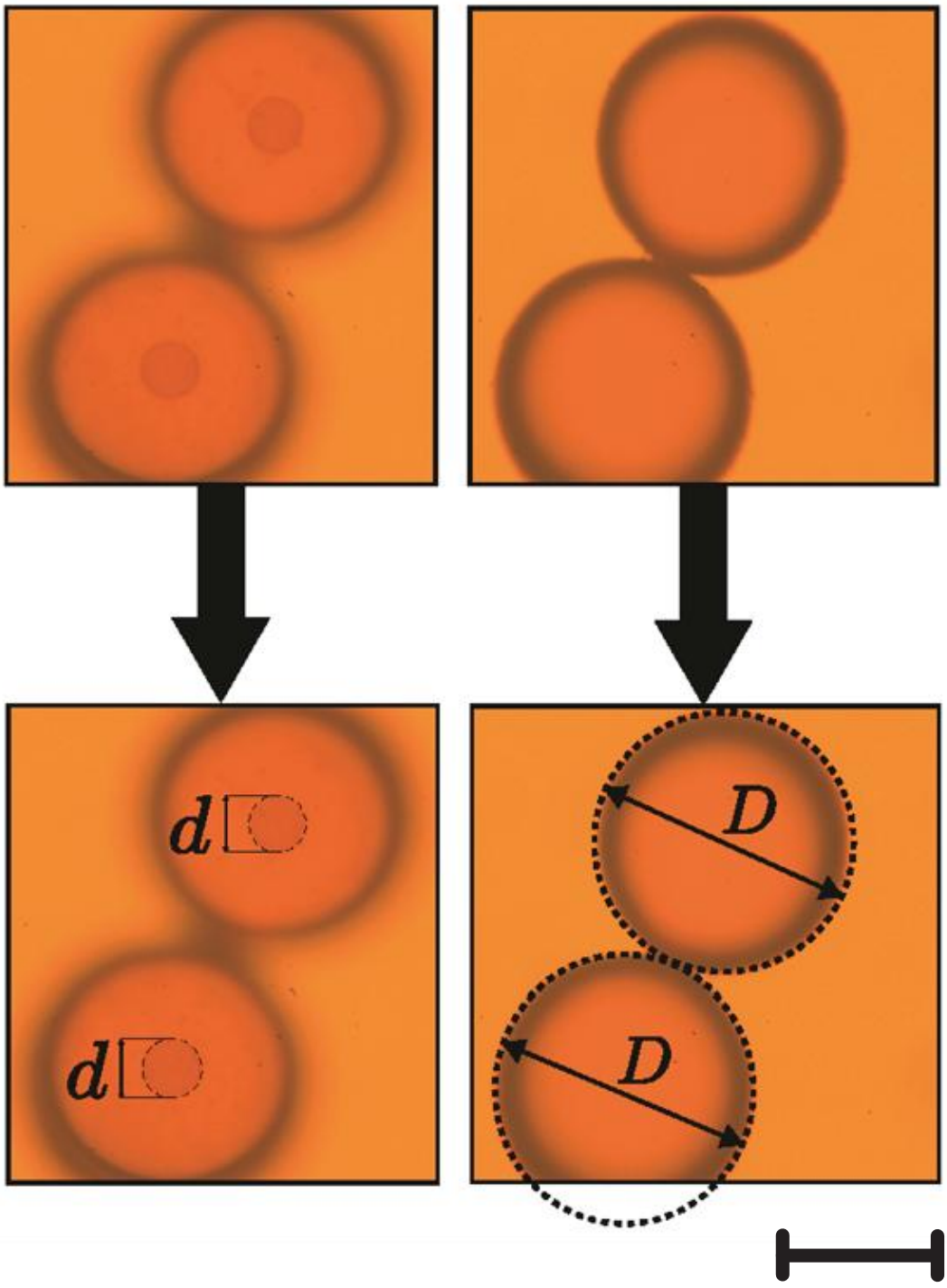

Figure S4: Illustration of measurement procedure for particle and patch diameters (D and d) for calculation of the $\beta_m = d/D$ parameter. To avoid errors due to non-telecentricity of the optics, separate images are taken focused on respectively the patch (left image) and the particle equator (right image) from with the two diameters are obtained. Particles are 75–90μm diameters particles with nominal $n_2 \approx 1.9$. The scale bar is 50 μm.

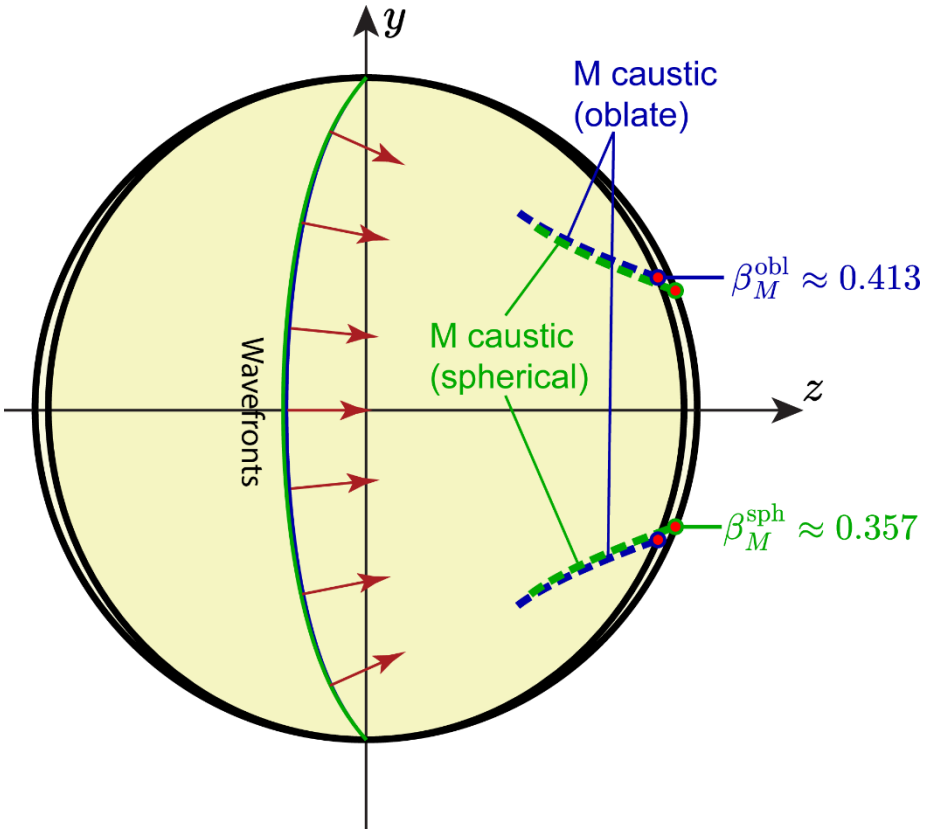

Figure S5: Ray tracing model of plane waves incident on a sphere and a 4% flattened oblate spheroid, showing the locations of the M-caustics as dashed green lines for the sphere and dashed blue lines for the oblate spheroid. Index constrast $m = 1.335$. For visual clarity, wavefronts propagated to the xy-plane (green and blue solid lines) are shown instead of individual rays. Comparing the two cases, we note that the flattening produces a 16% increase in β_M.

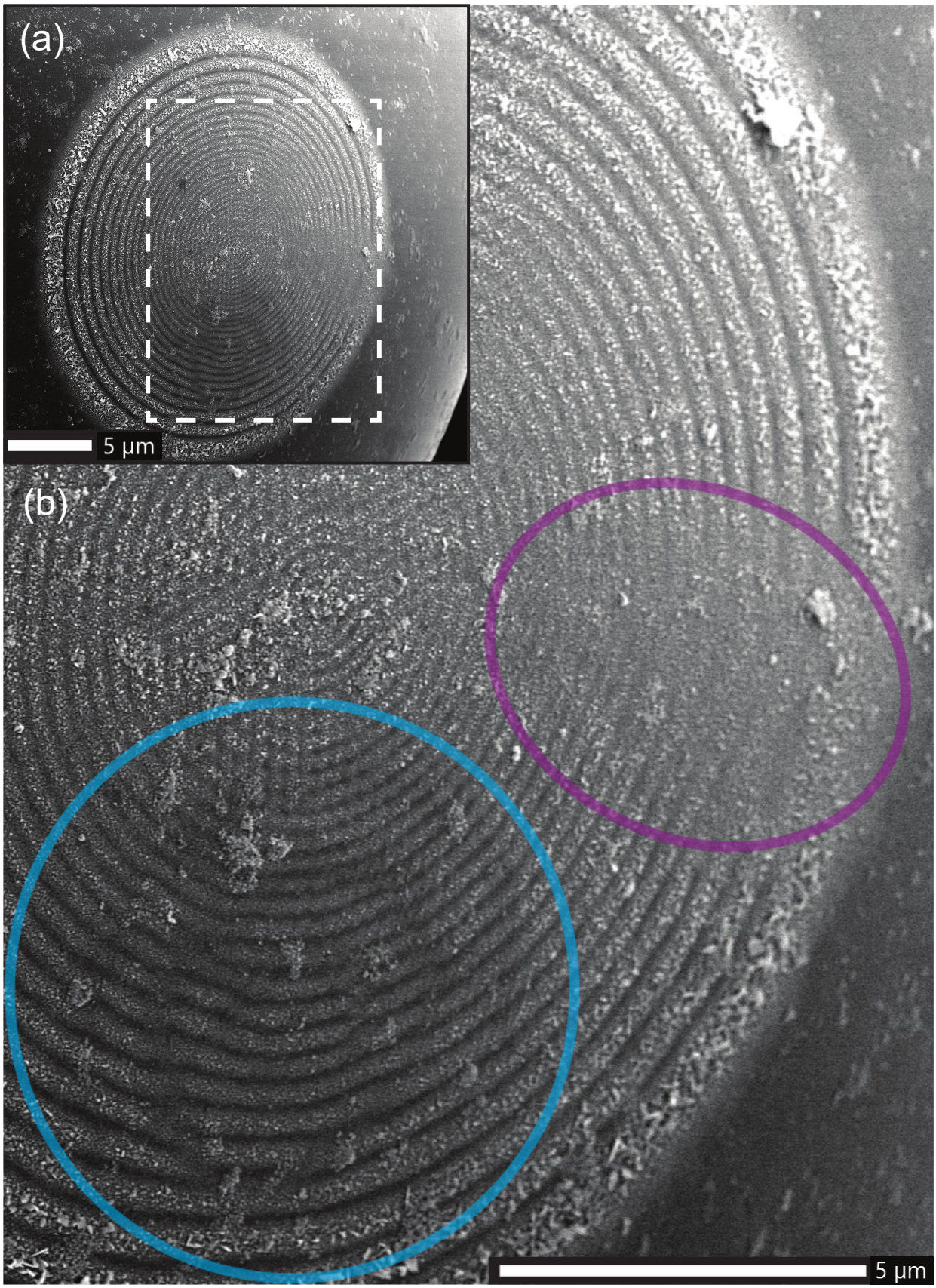

Figure S6: a) Overall patch image of particle shown in Fig. 8f,h. Distortion of the spot is evident inside of the white box which is magnified in b): Blue circle: Distortion of fringes, including broken and merging fringes. Purple ellipse: Washed-out fringes due to particle imperfections.

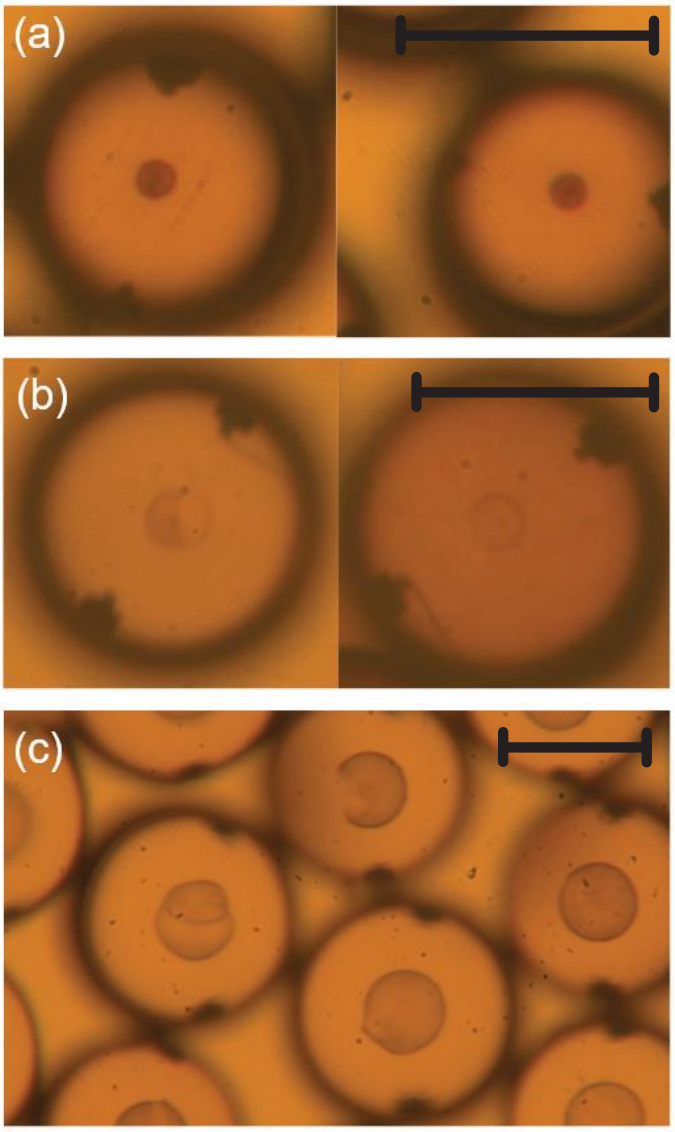

Figure S7: Examples of distorted patches deformed due to non-uniformity or non-sphericity of the particles.

a) $n_2 \sim 2.2$ particles with ∅ = 56–66 μm exposed in a 40%/60% DMSO/water mixture. Both particles are from the same experiment, with the left particle patch showing a small but clear deviation in size and shape compared to the typical particle patch appearing in the right patch.
b) $n_2 \sim 2.2$ particles with ∅ = 56–66 μm exposed in a 40%/60% DMSO/water mixture. The particles are from two separate experiments performed under the same conditions. Deviations from a round patch are clear in both cases, with the left patch exhibiting an area of missing deposition.
c) $n_2 \sim 1.9$ particles with ∅ = 75–90 μm exposed in 100% DMSO solvent. A relatively large fraction of particles in this batch are non-uniform, which is reflected in deformations of patches in nearly all the depicted patches.

All particles were coated with PDA and exposed to 405 nm wavelength light in 50 mM $AgNO_3$ solutions. The peripheral features in each particle are shadows from microfluidic ports present in an earlier version of the microfluidic cell. The scale bars are 50 μm.

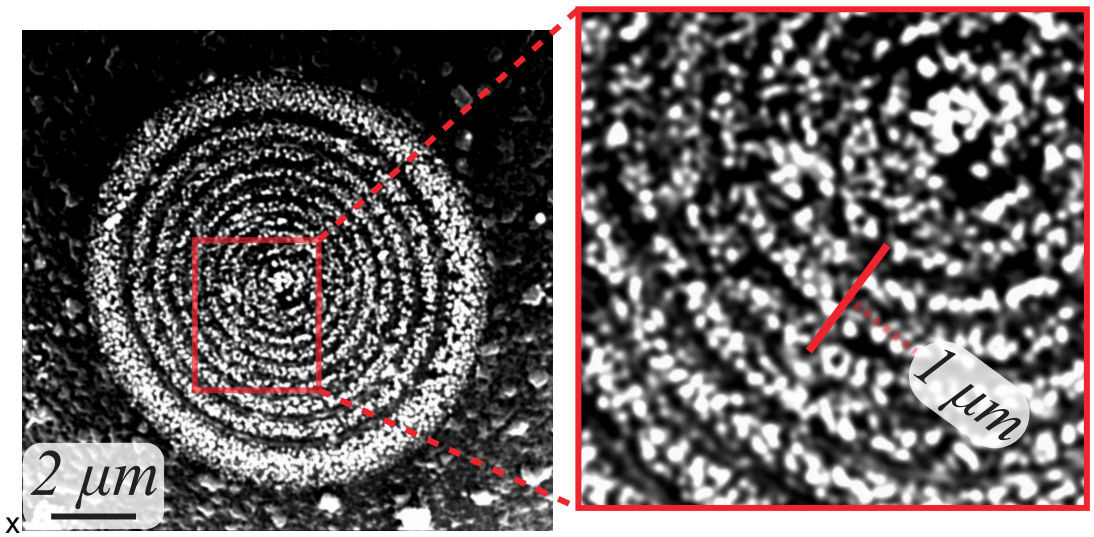

Figure S8: Image showing the resolution of fringes on a PDA-Functionalized BTG microsphere, nominal n = 2.2 exposed in 100% DMSO. 4 discernable fringes are displayed across a 1 μm distance, so the spatial resolution of the pattern can be estimated to be .33 μm or better.

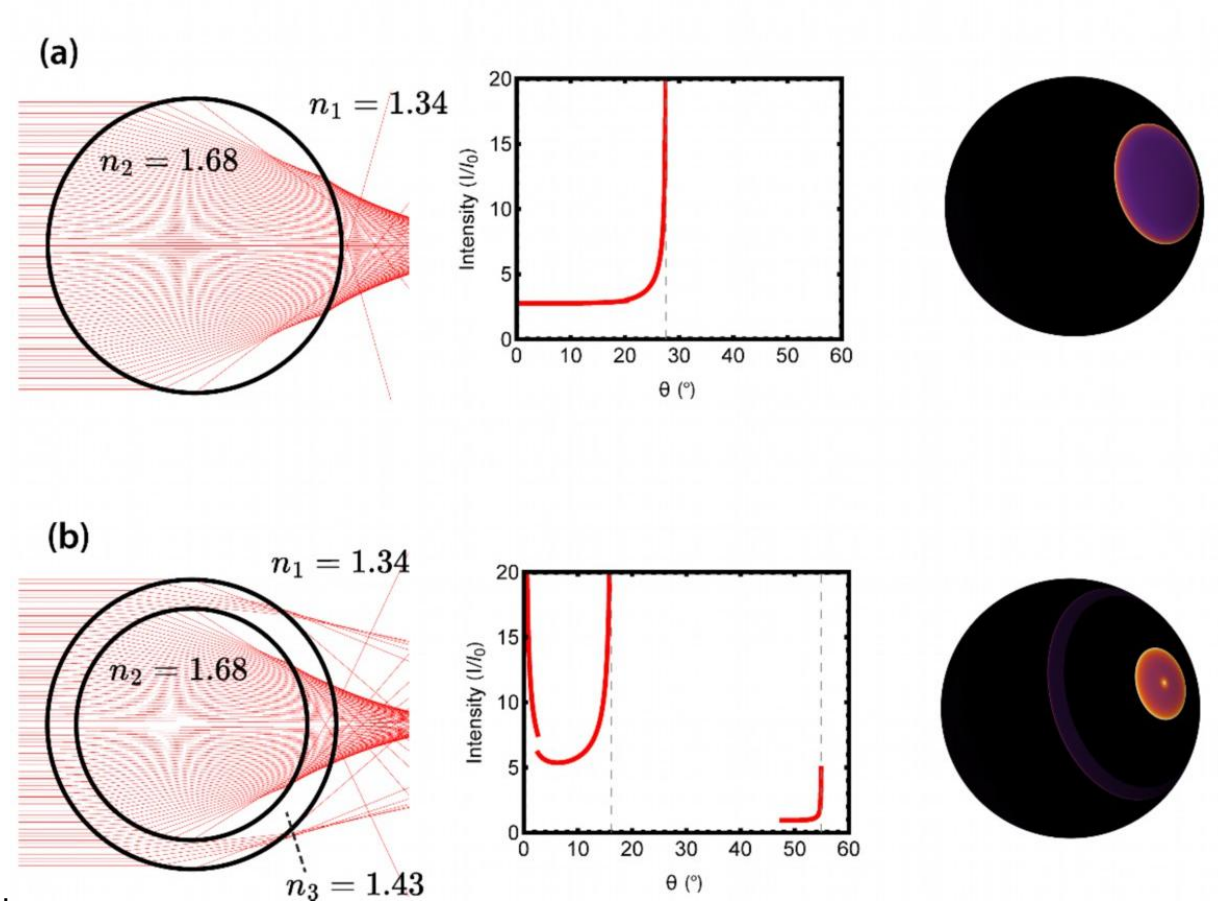

Figure S9: Simulations of μSAL patch formation in (a) a uniform sphere with refractive index $n_2 = 1.68$ immersed in water and (b) a core/shell dielectric sphere with core (80% of radius) refractive index of $n_2 = 1.68$ and shell (20% of radius) refractive index of $n_2 = 1.43$. The patches cover solid angles of approximately $\frac{4\pi}{18}$ sr in the uniform sphere and $\frac{4\pi}{51}$ sr in the core/shell particle.